PHYSICAL REVIEW B VOLUME 30, NUMBER 4 15 AUGUST 1984

Electronic structure of hydrogenated and unhydrogenated amorphous SiN_x ($0 \leq x \leq 1.6$): A photoemission study

R. Kärcher, L. Ley, and R. L. Johnson
Max-Planck-Institut für Festkörperforschung, Heisenbergstrasse 1, D-7000 Stuttgart 80, Federal Republic of Germany
(Received 27 February 1984)

We present a comprehensive core-level and valence-band photoemission study of hydrogenated and unhydrogenated amorphous silicon nitride (a-SiN_x:H and a-SiN_x). Position, width, and shape of the Si $2p$ line as a function of x are interpreted in terms of a superposition of five chemically shifted components which correspond to the possible Si-$Si_{4-n}N_n$ ($n=0,\ldots,4$) bonding configurations. The chemical shift per Si—N bond is between 0.62 ($x \leq 0.6$) and 0.78 eV ($x \simeq 1.3$). From the intensities of the chemically shifted Si $2p$ components the number of Si—N bonds is calculated and compared with the total nitrogen concentration. Above $x \simeq 0.8$ the average number of N—Si bonds per N starts to deviate from three. The addition of hydrogen increases this deviation because N—H bonds are favored over N—Si bonds. A band of N $2p$ lone-pair states is identified at the top of the valence bands in nearly stoichiometric a-Si_3N_4. This band determines the position of the valence-band maximum (VBM) above $x=1.1$. Below $x=1.1$ Si—Si bonding states mark the VBM. The conduction-band minimum (CBM) is determined by Si-Si antibonding states up to $x=1.25$ and its position relative to the core levels is virtually unaffected by the presence of nitrogen or hydrogen. Above $x=1.25$, a transition to Si-N antibonding states occurs which is accompanied by a sharp recession of the CBM. The position of the Fermi energy within the gap is investigated as a function of x and the hydrogen content. Si—H and N—H bonding states are identified at 6.3 and 9.8 eV below the VBM in nearly stoichiometric a-Si_3N_1:H. Si—Si bonding defect states lie 0.5 to 1.0 eV above the VBM and the corresponding antibonding states (3.0 ± 0.3) eV above the VBM. Plasmon energies vary between 17 eV in a-Si and 22 eV in a-$SiN_{1.5}$.

I. INTRODUCTION

Silicon nitride (Si_3N_4) is used widely in microelectronics, e.g., as a passivation layer,[1] as an alkali-ion—diffusion barrier,[1] and as an insulator in thin-film transistors.[2] The material is also the key ingredient in nonvolatile memory elements based on metal-nitride-oxide-semiconductor field-effect transistors (MNOS FET's).[3,4] The write-and-erase operations involve the charging and discharging of trap states in Si_3N_4.[5] The same charge-storage capability is also used to induce a highly conductive inversion layer at the silicon surface in the metal-insulator-semiconductor inversion-layer (MIS IL) solar cell.[6] There is extensive literature on the charging and decharging of these trap states based on various models for the trap distribution and charge transport,[3,4] but experimental information on the energy distribution and the microscopic nature of the trap states is scarce. The only established fact is the presence of Si dangling bonds which give rise to an ESR signal with a g value of 2.0055, whereas a corresponding nitrogen-related signal appears to be absent.[7–9]

The characterization of defect states in silicon nitride is complicated by the preparation process: The material is deposited as a thin amorphous film either by glow-discharge (GD) decomposition of SiH_4+NH_3 (deposition temperature $T_D \simeq 300\,^{\circ}C$) or by the thermal decomposition ($T_D \simeq 500-1000\,^{\circ}C$) of silicon- and nitrogen-containing gases [chemical vapor deposition (CVD)].[1] Both methods yield, depending on the deposition conditions, nonstoichiometric specimens[10,11] and/or a gradient in the [Si]/[N] concentration ratio near the interfaces[12,13] with measurable differences in trap density and conductivity.[11,14,15]

In addition, both preparation methods introduce atomic hydrogen, as evidenced by the ir absorption corresponding to the Si—H and N—H stretching modes around 2220 and 3300 cm^{-1}, respectively.[16,17] Hydrogen concentrations between about 20 and 40 at. % (Refs. 10 and 18–20) have been measured in the low-temperature GD material and between 6 and 8 at. % in the high-temperature CVD material.[17,19] Recalling the profound effect hydrogen has in passivating defects in amorphous silicon (a-Si), it comes as little surprise that hydrogen reduces the midgap density of states (DOS) in a-Si_3N_4 as well.[9] Thus, any realistic calculation of the defect states in amorphous silicon nitride has to take into account the possibility of nonstoichiometry and the presence of hydrogen bonds. Robertson[21,22] has calculated local densities of states of Si dangling bonds, and Si—H and Si—Si bonds, and finds that the σ states of some of these configurations lie in the gap of Si_3N_4 and are therefore candidates for the trap states in the devices mentioned previously. The starting point in these calculations is the band structure of the crystalline β-Si_3N_4 modification, which has also been calculated with quite similar results by Ren and Ching.[23] The choice of β-Si_3N_4 as the model structure for amorphous Si_3N_4 is justified by the close similarity in short-range order, bond distances, and bond angles (see Table I) of the two forms of silicon nitride.[24,25] The structure follows the $8N$ octet rule: Silicon atoms are nearly

 ©1984 The American Physical Society

TABLE I. Bond angles and bond distances in different forms of Si_3N_4.

	Bond length (Å)	Spacing (Å)		Bond angles (deg)		Ref.
	Si—N	N—N	Si—Si	Si—N—Si	N—Si—N	
CVD a-Si_3N_4	1.729	2.83	3.01	121	109.8	25
CVD a-Si_3N_4	1.75		3.0			24
β-Si_3N_4	1.73—1.745	~3.0[a]	3.01	122—115		b

[a]Average of nonequivalent N positions.
[b]S. Wild, P. Grieveson, and K. H. Jack, in *Special Ceramic 5,* edited by P. Popper (British Ceramic Research Association, London, 1972), p. 385.

tetrahedrally surrounded by four nitrogen atoms and each nitrogen occupies a planar, triply coordinated site with Si as nearest neighbors. The symmetry of the planar site (D_{3h}) implies that the highest occupied states in Si_3N_4 are lone-pair orbitals of N $2p_z$ character.[21] Kirk suggested that Si_3N_4 could therefore have gap states with a negative effective correlation energy analogous to the situation in other lone-pair semiconductors[26] and he proceeded to suggest a mechanism for bulk charge storage, fatigue, and recovery in terms of these defects.[27] However, an early attempt to identify the nonbonding lone-pair states at the top of the valence bands in photoemission spectra of CVD Si_3N_4 was inconclusive.[28]

It is the purpose of our investigation to determine, by means of photoelectron spectroscopy (PES), the density of occupied states in a-SiN_x for a wide range of compositions from $x=0$ to 1.6. Deviating considerably from stoichiometry ($x=\frac{4}{3}=1.33$) puts us in the position of determining the energies of "wrong bonds," i.e., in particular, Si—Si bonds, and to make contact with a number of investigations dealing with the influence of small nitrogen concentrations on the transport properties of amorphous silicon.[8,16,29–32] By the deliberate and controlled incorporation of hydrogen, changes in the electronic structure of amorphous SiN_x due to the formation of Si—H and N—H bonds could be identified. Finally, by analyzing the chemical shifts of the Si and N core levels, we have settled the question of whether nonstoichiometric silicon nitride is a mixture of a-Si and a-Si_3N_4,[33] in favor of the random-network model as suggested by Philipp.[34] A preliminary report of these results has been given at the Tenth International Conference on Amorphous and Liquid Semiconductors.[35]

II. EXPERIMENTAL DETAILS

Photoelectron spectra of the valence bands were measured with a resolution of 0.3 eV using He I (21.12 eV) and He II (40.8 eV) excitation and synchrotron radiation in the range from 20 to 140 eV. X-ray-induced valence-band and core-level spectra [x-ray photoelectron spectroscopy (XPS)] were obtained with monochromatized Al $K\alpha$ radiation ($h\nu=1486.6$ eV), which gave an overall resolution of 0.86 eV. For the analysis of the Si $2p$ chemical shifts, high-resolution spectra [0.3 eV full width half maximum (FWHM)] of the Si $2p$ core levels were recorded for $110 \leq h\nu \leq 200$ eV, utilizing synchrotron radiation from the DORIS storage ring in Hamburg. The monochromator used is of the plane-grating type and the electron energy was measured with a cylindrical mirror analyzer set with its axis at 45° relative to the sample normal. Details of the apparatus have been published elsewhere.[36]

Hydrogen-free silicon nitride films were prepared by dc-sputtering of a crystalline-Si target in a mixture of argon and nitrogen. By adding H_2 to this mixture, up to ~10 at. % of hydrogen could be incorporated in the film. Higher hydrogen concentrations (~30 at. %) were achieved in specimens prepared by glow-discharge decomposition of SiH_4/N_2 gas mixtures. The deposition temperature of all films was room temperature, but provisions were made to anneal some samples between measurements up to 600 °C.

All of the specimens were prepared in special preparation chambers attached directly to the different spectrometers used so that the films could be transferred under UHV conditions from the deposition site to the measuring position. The spectra presented below are thus from specimens that contain no measurable (with PES and Auger-electron spectroscopy) concentrations of elements other than Si, N, and—if so desired—H. The nitrogen content of each film was determined from the intensity ratio of the N $1s$ to Si $2p$ core levels as measured by XPS. The method was calibrated with a Si_3N_4 sample whose stoichiometry was confirmed to within 5 at. % by atom-emission spectroscopy. For this sample, we obtained $I(\text{N } 1s)/I(\text{Si } 2p)=1.95\pm0.05$. After correction for differences in electron mean free paths and analyzer efficiency according to Ref. 37, we deduce a ratio of photoemission cross sections $\sigma(\text{Si } 2p)/\sigma(\text{N } 1s)$ of 0.51 at $h\nu=1486.6$ eV. This value compares well with the calculated ratio of 0.45.[38,39]

III. RESULTS AND DISCUSSION

A. Core levels

Binding energies relative to the Fermi level E_F and the widths of the Si $2p$ and N $1s$ core levels are plotted as a function of the nitrogen content x for a series of a-SiN_x films in Fig. 1. The binding energy of the Si $2p$ level increases monotonically from 99.60 eV in a-Si to 102.80 eV in a-$SiN_{1.5}$. This 3.2-eV increase in binding energy is accompanied by a gradual increase in the width of the line up to a maximum value of 2.8 eV around $x=0.7$. The

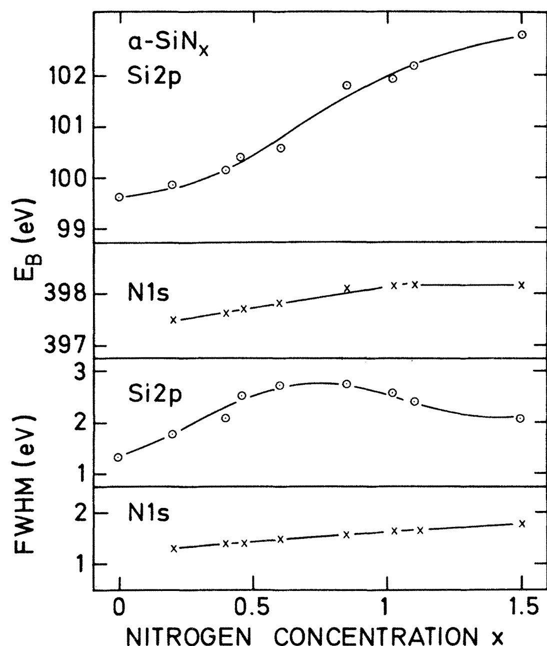

FIG. 1. Binding energy (relative to E_F) and width of the Si $2p$ and N $1s$ core levels of a-SiN_x as a function of x. The data were obtained from Al $K\alpha$ spectra recorded with a resolution of 0.86 eV. E_B refers to the binding energy of the peak maximum.

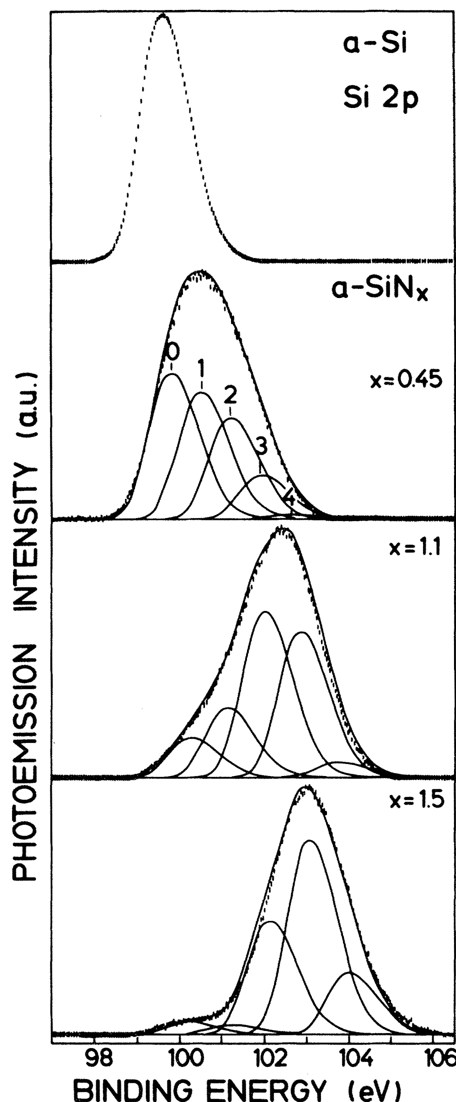

FIG. 2. Si $2p$ core-level spectra excited with Al $K\alpha$ radiation. The experimental points are fitted (method A) to a total of five equidistant peaks (solid lines), as explained in the text. (In subsequent figures, a.u. denotes arbitrary units.)

line narrows again for higher nitrogen concentrations without reaching the initial value of 1.3 eV (FWHM). Closer inspection of the line shape (see Fig. 2) reveals that the broadening is asymmetric with a distinct tailing towards higher binding energies for $x \lesssim 0.7$ and towards lower binding energy for $x \gtrsim 0.9$. In addition, we observe a structure around 100 eV binding energy in the form of a shoulder in the spectra of $SiN_{1.1}$ (compare Fig. 2). The binding-energy shifts of the N $1s$ level are in the same direction as those of the Si $2p$ line, but are small in comparison—only 0.6 eV between $x=0.2$ and 1.5—and the broadening amounts to a mere 0.5 eV. A maximum in the width of the N $1s$ level for intermediate nitrogen concentrations or any asymmetry in the line shape is not observed.

We interpret the Si $2p$ core-level spectra in terms of a superposition of chemically shifted components. Starting with the a-Si network in which each Si atom is surrounded by four other Si atoms as nearest neighbors, an increasing number of the homopolar Si—Si bonds are replaced by heteropolar Si—N bonds as nitrogen is added to the network. The charge transfer from Si to the more electronegative N leaves a positive charge on the Si atom, which results in a shift of all Si core levels towards higher binding energy. We thus expect five principal chemically shifted components—Si_0,Si_1, . . . , Si_4—corresponding to Si atoms where zero, one, two, three, or all four Si—Si bonds have been replaced by Si—N bonds. We have fitted the Si $2p$ spectra of SiN_x on the basis of this model. Since the individual Si_n ($n=0,\ldots,4$) components are not resolved, even in the spectra with the highest resolution (0.3 eV FWHM), three simplifying assumptions had to be made in order to keep the number of adjustable parameters to a minimum.

(i) We consider only the five principal lines Si_0, . . . , Si_4 referred to above.

(ii) The line shape is the same for each component.

(iii) The lines are equally spaced.

The last point is a consequence of the additivity of chemical shifts, which is also referred to as the concept of group chemical shifts.[40,41]

The first point is the most serious limitation. It means that we neglect induction effects, i.e., the influence of the second coordination shell on the chemical shifts. It has been shown theoretically[42] and experimentally,[43] for instance, that the charge transfer from Si to O in SiO_2 depends sensitively on the Si—O—Si bridging bond angle. A similar result might be anticipated for the Si—N—Si pyramidal angle even though, to our knowledge, no pertinent

calculations are available as yet. Spectroscopically, the induction effects distribute the intensity of each principal component Si_n among a number of sublevels with slightly different binding energies, depending on the atomic arrangement in the second coordination sphere. A case in point is the symmetrical line broadening observed in *a*-Si, which is due to small charges of both polarity on the Si atoms as a result of statistical fluctuations in second-nearest-neighbor distances around its mean value and the resulting distribution of chemically shifted Si core lines.[44] This example illustrates that the small chemical shifts connected with the induction effects cannot usually be resolved and may thus be taken into account by allowing for a certain broadening of the principal components. Experimentally, we find that the Si $2p$ line in a high-temperature CVD sample is 1.9 eV wide (FWHM), compared to 1.3 eV in *a*-Si. The additional broadening of 0.6 eV is, incidentally, comparable to the 0.5-eV value measured for the N $1s$ line between $SiN_{0.2}$ and $SiN_{1.5}$. If Si—N—Si bond-angle variations are mainly responsible for the broadening, we expect comparable charge fluctuations on Si and N atoms that are centered around the charges dictated by the ionicity difference of the two species forming the heteropolar bond. It is obvious that the data do not allow a detailed investigation of these effects. Instead, we have explored their influence on the fit parameters by considering two extreme situations. In fit *A* we set the line shape of all five components equal to that measured in pure *a*-Si. In fit *B* the Si $2p$ spectrum broadened to a width of 1.9 eV (FWHM) by folding it with a Gaussian is used as the fixed line shape. Free parameters were, in both cases, the line separation ΔE_N, i.e., the chemical shift per Si—N bond, and the relative intensities of the five components. Selected results of fit *A* in Fig. 2 illustrate that the asymmetric broadening and the energy shift of the Si $2p$ spectrum with the addition of nitrogen is well reproduced by the transfer of spectral weight from Si_0 to Si_n configurations. An equally satisfying reproduction of the data is achieved with fit *B*. The main difference is evident in the high-x spectra of Fig. 3: According to method *B*, comparable contributions to the experimental line shape come from Si-N_3 and Si-N_4 configurations, whereas method *A* yields Si—N_3 as the main configuration. This follows from the fact that the chemical shift per Si—N bond, E_N, obtained in fit *A*, is greater than that obtained in procedure *B*. ΔE_N is plotted as a function of x in Fig. 4. As expected, ΔE_N lies generally lower in fit *B* than in fit *A*. We also find that ΔE_N increases, in both cases, with the nitrogen content of the samples. A similar increase in the Si $2p$ shift of Si-O_4 units from ~ 3.5 to 4.1 eV was explained in terms of different extra-atomic relaxations for Si-O_4 dispersed in a silicon matrix and Si-O_4 in bulk SiO_2.[45] The data of Fig. 4 indicate that the ability of the network to provide some of the charge necessary to screen the core hole created in the photoemission process diminishes with the addition of nitrogen, as does the relaxation energy, which reduces the core-level binding energy. As a result, ΔE_N increases with x. This variation in ΔE_N reflects thus differences in the dielectric response of the medium and not an increase in the charge transfer with the addition of more Si—N bonds.

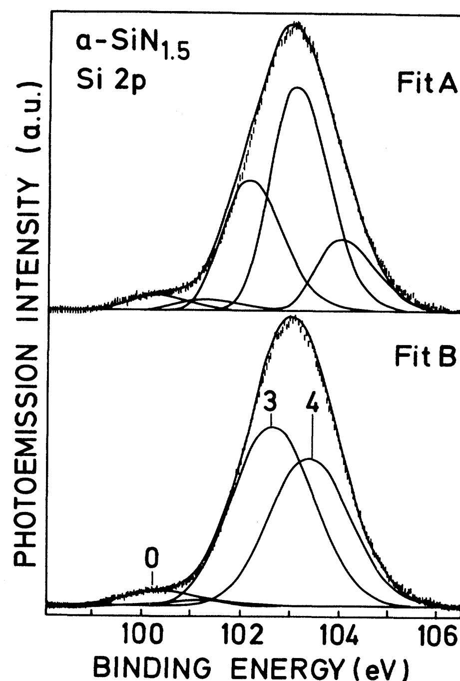

FIG. 3. Results of two different fitting procedures (see text) applied to the Si $2p$ core-level spectrum of *a*-$SiN_{1.5}$.

Which of the two curves in Fig. 4 should be considered as being representative of the chemical shifts in *a*-SiN_x? Considering what we said about the relationship between the widths of the N $1s$ and Si $2p$ core levels as a result of the induction effects, the dotted line in Fig. 4 is likely to be a more realistic estimate than any one of the two curves connecting the fit results. For small x, fits with a narrow line shape are most realistic, and, for high x, the broad peaks are clearly superior because they place most of the Si atoms in Si-N_4 environments, as expected. The dotted line interpolates smoothly between the two extremes and we may summarize the results as follows: For

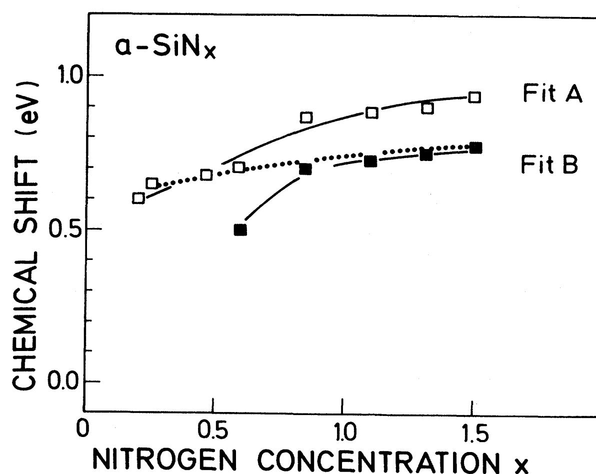

FIG. 4. Si $2p$ chemical shift per Si—N bond plotted as a function of x for the two fit procedures *A* and *B* described in the text.

isolated Si—N bonds in an amorphous silicon network the Si $2p$ binding-energy shift per Si—N bond is $\Delta E_N = (0.62\pm0.05)$ eV, and for the same bond in near-stoichiometric Si_3N_4, ΔE_N amounts to (0.78 ± 0.05) eV. These values lie between those derived for Si—O (0.9—1.1 eV) and Si—C (0.5 eV) bonds, as expected on the basis of the electronegativity of N (3.1), which is intermediate between that of O (3.5) and C (2.5).[46]

Our discussion so far has been based on the continuous random-network model for the structure of a-SiN_x. The description of nonstoichiometric silicon nitride (i.e., a-SiN_x for $x\neq\frac{4}{3}$) in terms of a mixture of a-Si and a-Si_3N_4, as proposed by Coleman and Thomas,[33] can be excluded on the basis of the Si $2p$ spectra alone. If their model were correct, all spectra would consist of only two lines separated by 2.5—3.0 eV, corresponding to Si atoms in a pure a-Si environment and to Si atoms in a-Si_3N_4 surrounded by four N atoms. This is clearly not what we observe.

From the intensity of the chemically shifted components $Si_1, \ldots, Si_4$, we can derive the concentration of nitrogen atoms bonded to Si. Let $x(\text{Si } 2p)$ be the number of nitrogen atoms bonded to silicon relative to all silicon atoms that contribute to the Si $2p$ core-level spectrum. $x(\text{Si } 2p)$ is given by[40]

$$x(\text{Si } 2p)=\frac{1}{3}\left[\sum_{n=1}^{4} nI(\text{Si}_n)\Big/\sum_{n=0}^{4} I(\text{Si}_n)\right], \tag{1}$$

where $I(\text{Si}_n)$ refers to the intensity of the Si_n component as obtained from the least-squares fit. The factor n in the numerator of Eq. (1) weights each component Si_n with the number of nitrogen atoms that give rise to that particular line, and the sum in the denominator is just the total number of silicon atoms contributing to the spectrum. The factor $\frac{1}{3}$ takes into account that each N atom is counted three times in Eq. (1), provided that the ideal threefold coordination with only Si as nearest neighbors is maintained throughout the concentration range studied. In Fig. 5 the values of $x(\text{Si } 2p)$ are plotted versus the absolute nitrogen concentration $x(\text{N } 1s)$ obtained as described in Sec. II. The straight line indicates the relationship expected if we were dealing with an ideal, fully coordinated network without "wrong" (i.e., N—N) bonds. The results for both fitting procedures are shown. As discussed earlier, the points from fit A (the open symbols in Fig. 5) are to be preferred for $x(\text{N}1s)\lesssim 0.6$, whereas for $x(\text{N } 1s) \gtrsim 0.8$ the results from fit B (the solid symbols in Fig. 5) give the more realistic estimate of $x(\text{Si } 2p)$. Up to $x=0.6$ the two concentrations $x(\text{N } 1s)$ and $x(\text{Si } 2p)$ track each other quite well for unhydrogenated samples, meaning that the data are in agreement with the ideal network structure as defined above. For $x(\text{N } 1s)\gtrsim 0.8$ the points start to deviate from the straight line, a trend which increases with increasing nitrogen content of the samples. The deviation is such that the amount of nitrogen bonded to Si, according to Eq. (1), is *less* than expected on the basis of the total nitrogen concentration $x(\text{N } 1s)$. We cannot dismiss the possibility of free nitrogen either in the form of N_2 molecules or atomic N, but it is more realistic to assume that a growing fraction of nitrogen atoms is either undercoordinated or has satisified some valencies by bonding to other nitrogen atoms. Both possibilities correspond to an effective N-Si coordination at a N site $C_{\text{Si}}(\text{N})$, of less than three. The value of $C_{\text{Si}}(\text{N})$ is obtained from the data of Fig. 5 according to

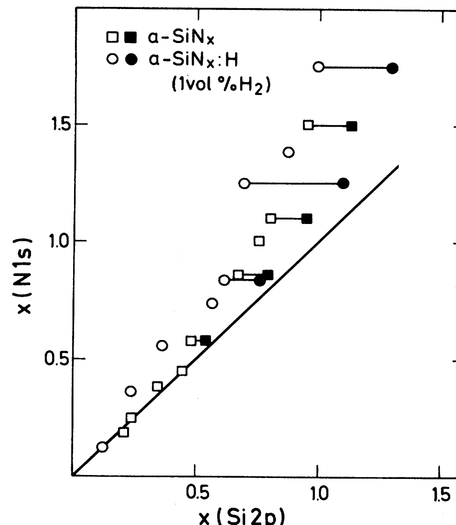

FIG. 5. Comparison of the nitrogen concentration $x(\text{N } 1s)$ calculated from the intensities of the N $1s$ and Si $2p$ core levels $x(\text{Si } 2p)$, the concentration deduced from the areas under the chemically shifted Si $2p$ lines as obtained in the two least-squares fits A (open symbols) and B (solid symbols).

$$C_{\text{Si}}(\text{N})=3x(\text{Si } 2p)/x(\text{N } 1s)\,. \tag{2}$$

For the sample closest to stoichiometric a-Si_3N_4, we obtain $C_{\text{Si}}(\text{N})=2.64$. This coordination number is similar to, albeit somewhat smaller than, the values of 2.72 and 2.78 deduced from x-ray- and neutron-diffraction experiments on high-temperature CVD material.[24,25] A higher defect density and, therefore, a lower effective coordination number in our low-temperature material, is expected according to the results of Aiyama *et al.*[24]

Nitrogen concentrations beyond $x(\text{N } 1s)=\frac{4}{3}$ require either undercoordinated nitrogen or homopolar N—N bonds, and this fact is evident by the larger deviations of $x(\text{Si } 2p)$ from the ideal-network line in Fig. 6. It is one of the results of our investigation, however, that these effects set in before the critical nitrogen content is reached. The question of whether nitrogen dangling bonds—possibly on inner-void surfaces as suggested by the authors of Refs. 24 and 25—or N—N bonds are the dominant defects cannot be answered on the basis of our data.

Figure 5 also includes films that were sputtered in N_2, Ar, and H_2 and therefore contain approximately 5—10 at. % hydrogen. The addition of nitrogen favors the incorporation of hydrogen, as was observed earlier by infrared spectroscopy.[20] We find that the incorporation of hydrogen generally increases the number of nitrogen atoms not fully coordinated by Si atoms, as illustrated by the fact that $x(\text{Si } 2p)$ in these films deviates more from the ideal line even for low x than the corresponding points for unhydrogenated specimens. Indeed, the highest nitrogen concentration, $x(\text{N } 1s)=2.0$, is only achieved with the

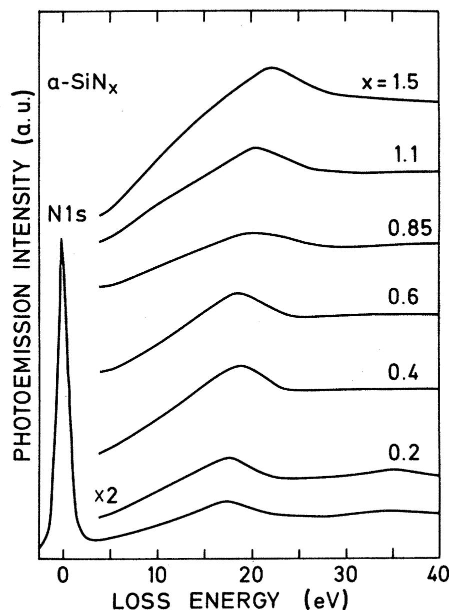

FIG. 6. Plasmon losses of the N 1s core line as a function of nitrogen content.

addition of hydrogen. We suggest, therefore, that the possibility of forming N—H bonds favors the incorporation of nitrogen into a-SiN$_x$.

So far we have concentrated on the Si chemical shifts and its implication for the structure of a-SiN$_x$. However, we also observe a shift of about 0.6 eV toward higher binding energy for the N 1s level between $x=0.2$ and 1.5 (cf. Fig. 1), as mentioned earlier. In an ideal-network structure of SiN$_x$, nitrogen is always fully coordinated by three Si atoms independent of the nitrogen concentration. We therefore expect no chemical shift that changes with x. Any incomplete coordination or the formation of "wrong" bonds with atoms more electronegative than Si, such as N or H, reduces the negative charge which resides on the N atoms due to the formation of the heteropolar N—Si bonds. This would induce, in principle, a chemical shift towards higher binding energies. We have determined the number of wrong or unsatisfied bonds for the near-stoichiometric sample of Fig. 5 as 0.36 out of three, or 12%. If only 12% of the spectral weight of a line is shifted to higher binding energies, we expect to see an asymmetry, a weak shoulder, or a small satellite, depending on the magnitude of the chemical shift, and not a displacement of the entire line as measured. We thus dismiss the possibility of chemical shifts as an explanation for the binding-energy variation of the N 1s line. Instead, we suggest that the N 1s shift reflects a shift of the Fermi level in the band gap of a-SiN$_x$ which should affect the binding energies (measured relative to E_F) of all core levels in the same way. We indeed find that the energy of the Si$_0$ component of the Si 2p spectra increases by the same amount, namely from 99.60 ($x=0$) to 100.20 eV in SiN$_{1.5}$, as seen in Fig. 2. These binding energies are independent of the ansatz used for the line shape in the fitting procedure. A Fermi-level shift is also in agreement with the results of the valence-band spectra (see Sec. III F where this aspect will be discussed further).

B. Plasmons

The XPS core lines are accompanied, on the high-binding-energy side, by loss maxima due to the creation of plasmons which are excited by the outgoing photoelectrons (see Fig. 6). The energies of the loss maxima increase from 17.0 eV in a-Si to 22 eV in a-SiN$_{1.5}$. There appears to be a small systematic ($\sim$0.4 eV) difference in the plasmon energies associated with the Si 2p and N 1s lines in the hydrogenated samples, while these energies agree well in the unhydrogenated samples (compare Fig. 7).

In the free-electron approximation the plasmon energy $\hbar\omega_p$ is given by

$$(\hbar\omega_p)^2=\frac{\hbar^2 4\pi e^2}{m}N_v \;, \tag{3}$$

where m is the electron mass. The valence-electron concentration N_v is related to the density ρ and the nitrogen content x according to

$$N_v=\rho\frac{n_{\rm Si}+xn_{\rm N}}{A_{\rm Si}+xA_{\rm N}}L_A \;. \tag{4}$$

The number of valence electrons and the atomic weight of Si and N are denoted by $n_{\rm Si}$ $(=4)$, $n_{\rm N}$ $(=5)$, and $A_{\rm Si}, A_{\rm N}$, respectively, and L_A is Avogadro's number. We have used this expression to derive the densities of our samples using the experimentally determined plasmon energies. The result (see Fig. 7) agrees reasonably, for $x=0$, with the known density of a-Si,[47] 2.1—2.3 g/cm^3. Above $x\simeq0.6$ the derived densities are substantially lower (between 5% and 20%) than those determined directly by other authors.[24,28] Electron-loss measurements[49,50] on

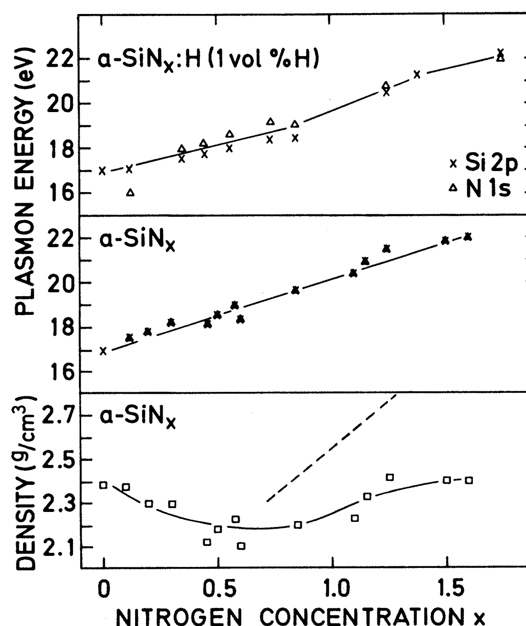

FIG. 7. Plasmon energies for a-SiN$_x$ and sputtered a-SiN$_x$:H deduced from the losses of the Si 2p and N 1s core-level spectra. The plasmon energies were used to calculate the densities of the samples as shown in the lower part. Measured densities (Ref. 48) are indicated by the dashed line.

samples prepared at higher temperatures, which are thus expected to have a higher density, yield plasmon energies comparable to ours. It thus appears that the relationship between density and plasmon energy based on the free-electron model does not hold rigorously in a-SiN_x.

C. Valence-band spectra of a-$Si_3N_{4.5}$

Figure 8 shows the valence-band spectra of a near-stoichiometric a-$SiN_{1.5}$ specimen prepared by sputtering (SP) as described in Sec. II. The spectrum excited with monochromatized Al $K\alpha$ radiation ($h\nu = 1486.6$ eV) was recorded with a resolution of 0.86 eV, whereas the spectrum labeled $h\nu = 87.1$ eV was measured with a resolution of 0.3 eV using synchrotron radiation. A comparison of the sharpness of the edges of the energy-distribution curves (EDC's) confirms that the energy resolution is not the limiting factor for the definition of structures in these spectra. The reference energy for the binding-energy scale, as in all following EDC's, is the Fermi level.

We distinguish two regimes in the EDC's of a-$SiN_{1.5}$. The 12-eV-wide upper portion of the valence bands consists primarily of states derived from Si $3s$, Si $3p$, and N $2p$ electrons. Separated from these by a gap of 3 eV, a single 4.5-eV-wide peak centered at $E_F - 20$ eV has almost exclusively N $2s$ character. The upper portion exhibits three maxima, labeled A, B, and C in Fig. 8, with binding energies of 4.9, 7.5, and 12.4 eV, respectively. All of these features are qualitatively well reproduced by the densities of states of β-Si_3N_4 calculated by Robertson[51] and Ren and Ching[23] also included in Fig. 8. The densities of states have been shifted in energy so that the mean position of the "N $2s$" states line up with the corresponding feature in the EDC's. Aside from some differences in the positions of the peak maxima, the main discrepancy appears to be an additional peak around 14.3 eV in the calculation of Robertson which is neither experimentally observed nor calculated by Ren and Ching.[23] The slight nonstoichiometry of our sample (compared to Si_3N_4) cannot be responsible for the lack of this peak since little change over a wide range of nitrogen concentrations is observed in the high-binding-energy portions of the EDC

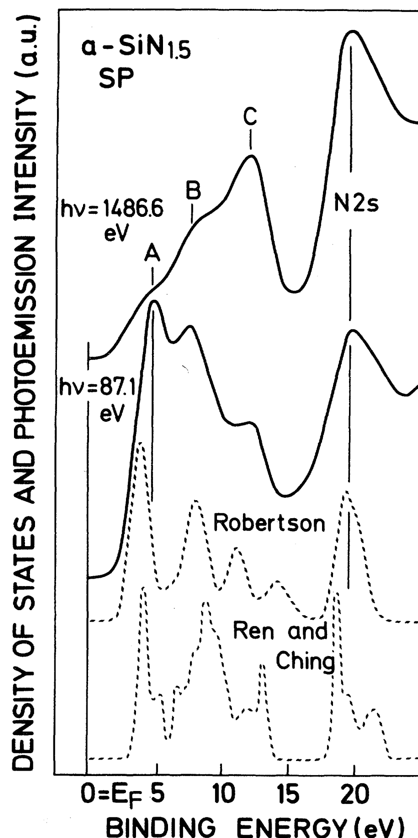

FIG. 8. Valence-band spectra of sputtered a-$Si_3N_{4.5}$ excited with monochromatized Al $K\alpha$ radiation ($h\nu = 1486.6$ eV) and with synchrotron radiation ($h\nu = 87.1$ eV). Also shown are densities of states calculated by Robertson (Ref. 51) and Ren and Ching (Ref. 23) for crystalline β-Si_3N_4.

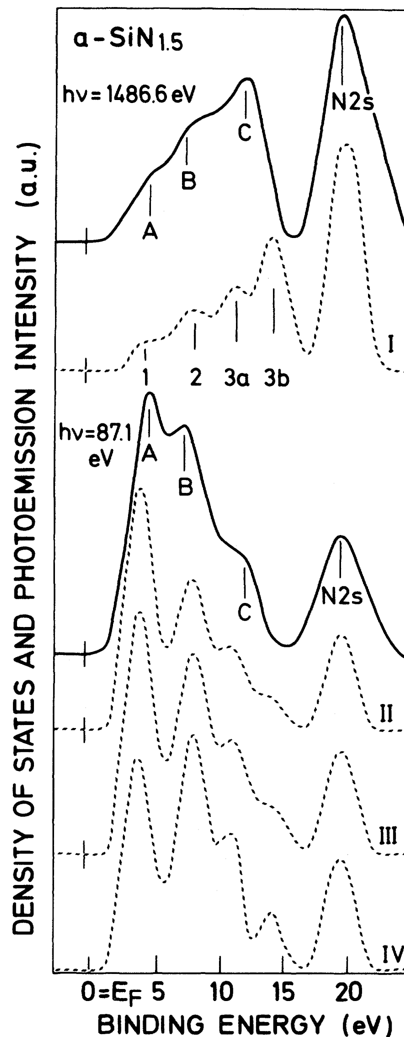

FIG. 9. Experimental EDC's corrected for a background of inelastically scattered electrons compared with theoretical EDC's obtained from the partial DOS's calculated by Robertson (Fig. 10) after weighting with the appropriate photoemission cross sections and broadening with a Gaussian of 2 eV FWHM (dashed lines I and II). The meaning of curves III and IV is explained in the text.

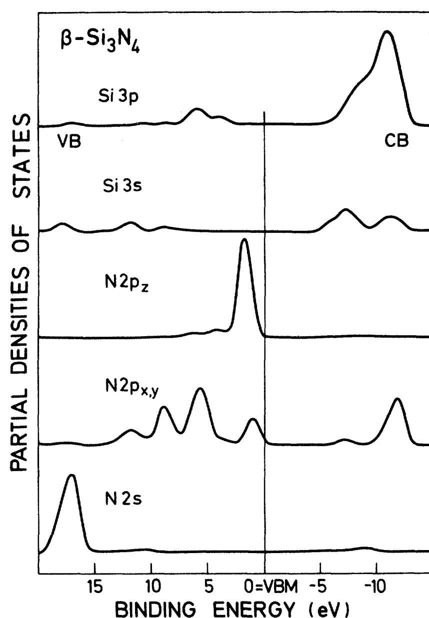

FIG. 10. Partial densities of states of β-Si_3N_4 calculated by Roberston (Ref. 51).

(see below). A quantitative comparison between the DOS and the EDC must take the photoemission cross sections into account. The striking reversal in the intensities of peaks *A*, *B*, and *C* in the two spectra of Fig. 8 are due to differences in the partial Si 3s, Si 3p, and N 2p cross sections. The descending order of intensities in the 87.1-eV spectrum is representative for all spectra between $h\nu=20$ and 120 eV, whereas the ascending order marks the high-photon-energy limit.

In Fig. 9 we compare the two spectra after correction for a background of inelastically scattered electrons with EDC's that have been synthesized from the partial densities of states of Robertson[51] (Fig. 10) after weighting them with the atomic photoemission cross sections as listed in Table II. The cross sections for the nitrogen states were obtained by interpolating between the values for oxygen and carbon calculated by Goldberg and Fadley.[52] In the energy range between 1486.6 and 132.3 eV the interpolated cross sections agree quite well with those calculated by Band *et al.*[38] for nitrogen. The interpolated N 2s cross section at $h\nu=1486.6$ eV was too large and had to be reduced by a factor of 3 to agree with the experimental data. The theoretical EDC's in Fig. 9 contain, in addition, correction factors of the order of unity to take into account the anisotropy of photoelectron emission with respect to the incident light and the collection geometry used. These asymmetry parameters were also taken from the work of Goldberg[52] and Band.[38] After adding the properly weighted partial densities of states they were folded with a Gaussian of 2 eV FWHM and the result is shown by the dashed lines labeled I and II in Fig. 9. The synthesized EDC's are seen to reproduce faithfully the spectra and, in particular, the changes in the relative intensities of the substructures. This implies that the partial densities (cf. Fig. 10) are likely to be correct and we can make the following assignment: peak *A* is the nonbonding N $2p_\pi$ lone-pair band. The contribution from N $2p_{x,y}$ states in this region is not more than 20%. Peak *B* has predominantly N $2p_{x,y}$ character with some contribution from Si 3p states. Peak *C* similarly comprises N $2p_{x,y}$+Si 3s electrons and the dispersion which leads to the splitting into 3a and 3b (see Fig. 9) in the DOS of Robertson is somewhat too large. The states around 20 eV binding energy are virtually pure N 2s. The bonding states which make up the valence bands are primarily nitrogen derived, whereas the weight of the conduction bands is carried by the Si states, as expected on the basis of the ionicities of the two elements.

Two things are to be learned from this comparison. First, the DOS of amorphous $Si_3N_{4.5}$ is seen to be well described by that of crystalline Si_3N_4, bearing witness to the fact that the DOS is essentially determined by the short-range order, i.e., bond angles, bond distances, and coordination number. Second, small deviations from stoichiometry seem to matter only slightly and those differences which might exist are covered by the $\sim$2-eV broadening due to the loss of long-range order. Most important, however, is the clear identification of a nitrogen-derived lone-pair band at the top of the valence bands. The lone-pair band is not as well separated from the remainder of the bands, as in SiO_2, presumably as a result of the smaller polarity of the Si—N bond.[53] As mentioned earlier, a strictly nonbonding N $2p_z$ state is only possible for N atoms in a planar configuration. While this situation appears to be realized *on the average* in a-Si_3N_4, fluctuations in the Si—N—Si bond angle about its ideal value of 120° make for a pyramidal arrangement followed by a mixing of p_z and $p_{x,y}$ states. Just what degree of $p_{x,y}$ admixture might be tolerated without destroying the agreement between calculated and measured EDC's was tested by adding Si 3p character to peak *A* at the expense of N 2p character and doing the opposite for *B*. Curves III and

TABLE II. Photoemission cross sections (in barns) used in the analysis of valence-band spectra.

$h\nu$ (eV)	H 1s	N 2s	N 2p	Si 3s	Si 3p
40.8	1.5×10^{6} [a]	9×10^{5} [b]	3.5×10^{6} [b]	3.4×10^{5} [b]	3.3×10^{5} [b]
87.1	7×10^{4} [a]	5.5×10^{5} [b]	1.1×10^{6} [b]	1.6×10^{5} [b]	1.8×10^{5} [b]
1486.6	3×10^{0} [a]	1.2×10^{3} [c]	1.3×10^{2} [c]	1.1×10^{3} [c]	1.9×10^{2} [c]

[a] J. A. R. Samson and R. B. Cairns, J. Opt. Soc. Am. 55, 1035 (1965); interpolated between the photon energies given.
[b] Reference 52; N 2p and N 2s interpolated between oxygen and carbon.
[c] Reference 38.

IV in Fig. 9 correspond to 20% and 40% contributions of Si $3p$ states to region A, respectively. It is clear that 20% may be tolerated, but 40% would lead to a reversal of the intensities of peaks A and B, in contrast to our finding. This admittedly crude test, which neglects any change in the energy eigenvalues, nevertheless indicates a certain tolerance of the measured spectra to the kind of rehybridization which is likely to be related to a reduction of the N-site symmetry from D_{3h} to C_{3h}.[21] The question of whether Si $3d$ states contribute to the stabilization of the planar N site cannot be answered by our spectra due to the low Si $3d$ partial cross sections.

D. Evolution of valence-band spectra of a-SiN$_x$ from $x=0$ to 1.6

In Figs. 11 and 12 we present the valence-band (VB) spectra of a series of sputtered a-SiN$_x$ specimens with increasing amounts of nitrogen and starting with pure amorphous silicon. We have chosen these two sets of spectra because emission from the N $2p$ states dominates in the He II spectra over the Si-derived states due to their higher photoemission cross sections. N $2p$ and Si $3p$ have comparable cross sections at $h\nu=1486.6$ eV and σ(Si $3s$) is a factor of 6 higher at this photon energy (compare Table II). The 4-eV-wide peak at the top of the a-Si VB seen in both sets of spectra is due mainly to Si $3p$ electrons. A second "hump" of Si $3s$ —derived states between 5 and 15 eV dominates the a-Si XPS spectrum of Fig. 12. Emission from these states contributes to the unstructured plateau between 5 and 15 eV in the He II spectrum (Fig. 11) that merges with the rising background at E_F-15 eV.[54]

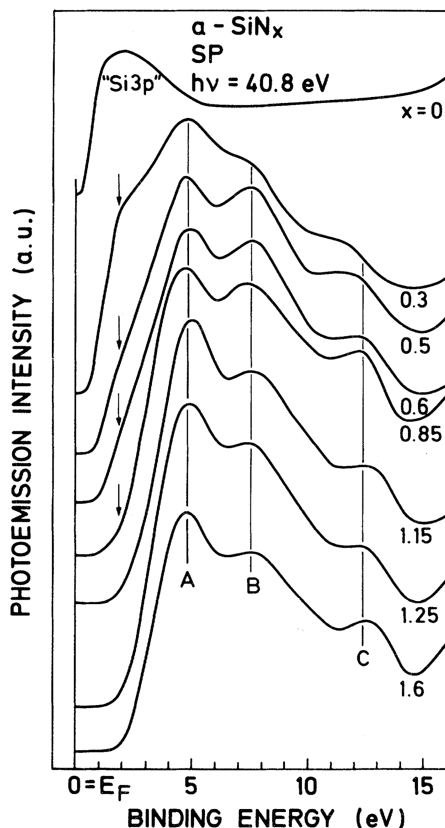

FIG. 11. He II valence-band spectra of sputtered (SP) a-SiN$_x$ films for $x=0$ to 1.6.

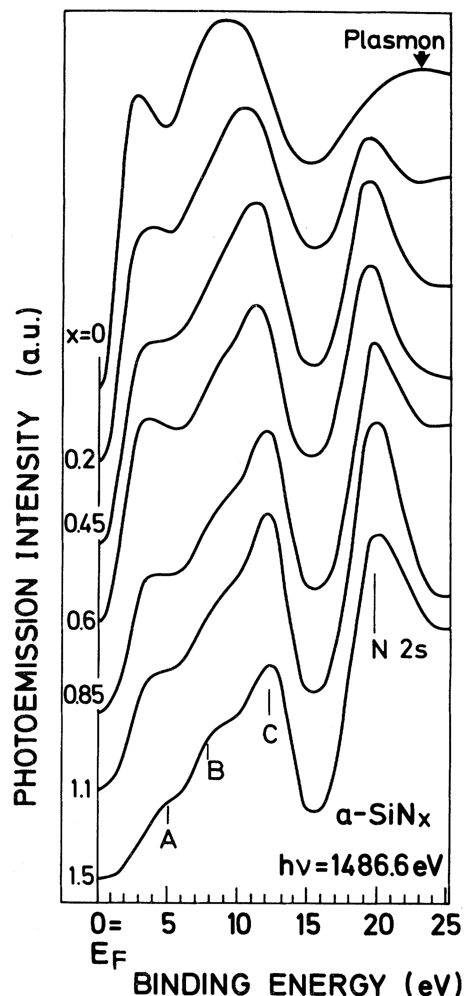

FIG. 12. Al $K\alpha$ valence-band spectra of sputtered a-SiN$_x$ films for $x=0$ to 1.5.

With the addition of nitrogen, the characteristic $A-B-C$ structure develops immediately in the 40.8-eV spectra. Above and including $x=0.6$ the energies of these structures are those of the nitrogen bonding states in Si_3N_4, as discussed in the preceding section. This means that the nitrogen is mainly in its proper N-Si$_3$ configuration, in agreement with the results of the analysis of the Si $2p$ chemical shifts in Sec. III A. Above $x=0.8$, small concentrations of undercoordinated nitrogen start to be incorporated into the network, as judged from the core-level spectra. This apparently has no influence on the valence bands unless we consider the 0.4-eV increase in the $A-C$ separation in a-SiN$_{1.6}$ as an indication of these irregular bonding configurations. For the films with $x=0.5$ and 0.3, the separation between A and C decreases by 0.5 and 1 eV, whereas peaks A and B remain unchanged at 4.9 and 7.5 eV below E_F. Isu and Fujiwara[55] observed a similar three-peak structure on a nitrided Si(111) surface: a peak at 4.2 eV and two shoulders

at 7.2 and 10 eV binding energy. Allowing for a 0.7-eV difference in the position of E_F, these values correspond to 4.9, 7.9, and 10.7 eV, in reasonable agreement with the a-$SiN_{0.3}$ spectrum. We can only speculate that the reduced $A-C$ splitting may have to do with a loss of the planar nitrogen environment.

In the XPS spectra of Fig. 12 the Si 3s partial density of states (PDOS) is emphasized due to its higher cross section at $h\nu=1486$ eV. This has the effect that the $A-B-C$ structure is only seen for the higher nitrogen concentrations. Below $x=0.6$ the prevailing Si PDOS develops gradually into that of the pure a-Si network.

The top of the valence bands (TVB's) in a-Si is made up of Si 3p bonding states. As small amounts of nitrogen are added to a-Si, these Si—Si bonding states remain at the TVB, up to $x=0.85$, as a shoulder which is marked by an arrow in Fig. 11. In XPS, Si 3p and N 2p states have comparable cross sections and the shoulder and peak A are not resolved. As a result, peak A appears to shift towards lower binding energy with decreasing nitrogen content (see Fig. 12). Below $x\cong 0.9$ the top of the valence bands in a-SiN_x is thus due to Si—Si 3p bonding states; above $x\cong 1.1$ the nitrogen lone-pair states determine the valence-band maximum (VBM).

The position of the shoulder in Fig. 11 remains fixed relative to peaks A and B and we can therefore assume that this situation also holds in stoichiometric a-Si_3N_4, where these states correspond to localized defects due to Si—Si bonds. The corresponding defect states thus fall in the lower half of the gap, approximately 0.4 to 0.5 eV above the VBM and about 1.7 eV below E_F. Robertson,[22] in his calculation, places the occupied Si-Si defect states 3 eV above the VBM, which appears to be too high compared with experiment.

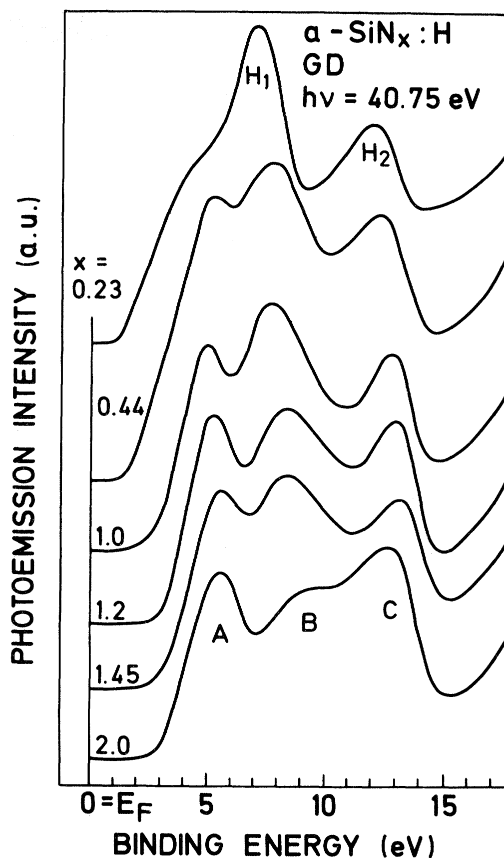

FIG. 13. Valence-band spectra of glow-discharge (GD) hydrogenated a-SiN_x:H films.

E. Valence-band spectra of hydrogenated a-SiN_x (a-SiN_x:H)

Amorphous SiN_x:H films sputtered with 0.1 and and 1 vol % H_2 in the sputter gas contain approximately 5 to 10 at. % hydrogen, respectively. The hydrogen content of glow-discharge specimens deposited from a mixture of SiH_4 and N_2 is in excess of 30 at. %. These concentrations are deduced from the intensities of the Si—H and N—H stretching bands in the infrared- (ir-) absorption spectra of the films using the proportionality factors of Ref. 17. Since no systematic investigations of the ir cross sections as a function of hydrogen and nitrogen content has been undertaken as yet, the concentrations must be considered very qualitative.

We shall discuss the influence of hydrogen on the DOS of a-SiN_x in connection with the 40.75-eV spectra of the GD samples of Fig. 13. The energies of hydrogen-induced states in sputtered a-SiN_x:H are identical, but they are less distinct due to the lower hydrogen concentration. The shape of the spectrum of a-$SiN_{0.23}$:H in Fig. 13 is quite similar to that of a-Si:H prepared at room temperature:[54] the two Si—H bonding states labeled H_1 and H_2 in Fig. 13 dominate the spectrum and the Si 3p states contribute the shoulder at $\sim E_F-4$ eV. The peaks H_1 and H_2 are characteristic for hydrogen bonded in polyhydride configurations such as Si—H_2, Si—H_3, or $(Si-H_2)_n$. Starting at $x=0.44$, peak A becomes discernible and H_1 and H_2 appear to develop into peaks B and C as the nitrogen content increases. We notice, however, that the intensities of peaks B and C relative to peak A are enhanced compared to the corresponding spectra of unhydrogenated a-SiN_x in Fig. 11. The extra spectral-weight shifts, furthermore, from peak B at low x to peak C for $x \gtrsim 1.2$. Si—H and N—H bonding states are apparently superimposed on peaks B and C and difference spectra are needed to distinguish between them. We note in passing that the nitrogen content of the last spectrum in Fig. 13 ($x=2.0$) is far greater than the amount which could be accommodated in a fully coordinated Si_3N_4 network. That the addition of hydrogen appears to increase the nitrogen concentration of a-SiN_x specimens under otherwise unchanged deposition conditions has also been observed by others.[56]

We have identified the hydrogen-related states on the basis of two kinds of difference spectra: those with and without hydrogen and those of hydrogenated films taken at different photon energies. Figure 14 shows the VB spectra of the GD a-SiN_2:H specimen using photon energies from 30.5 to 118.1 eV. The ratio of H 1s to N 2p, Si 3p, and Si 3s photoemission cross sections reaches its maximum around 30.5 eV, and σ(H 1s) is much smaller compared to the others above $\sim$85 eV (see Table II). This explains the variation in the intensity of peak C relative to

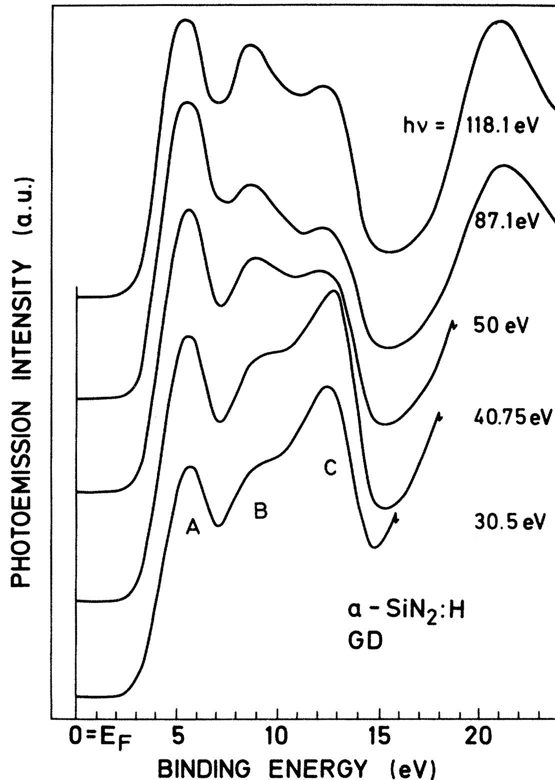

FIG. 14. Valence-band spectra of GD a-$SiN_{2.0}$:H as a function of photon energy.

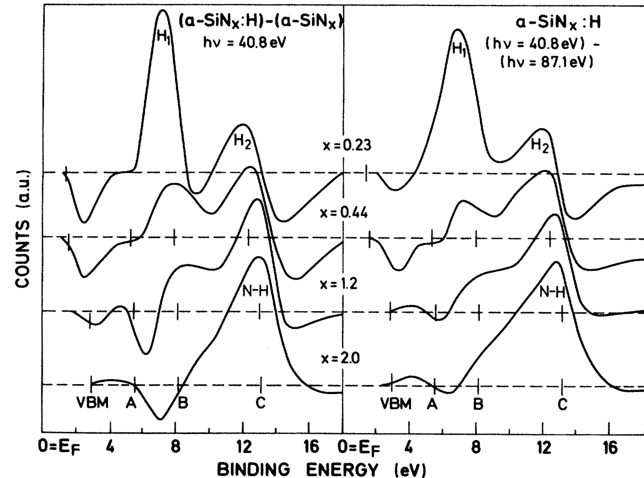

FIG. 15. Difference spectra of hydrogenated and unhydrogenated a-SiN_x films (left) and the difference between a-SiN_x:H spectra taken with two photon energies having widely differing H 1s photoemission cross sections (right).

A and B because H 1s states contribute mostly in the region C. The difference between the 40.75-eV spectrum and the 87.1-eV spectrum should thus give mainly the energy distribution of the partial H 1s—derived density of states. This method has the advantage that it compares spectra taken on the same specimen and it allows for an independent check on the conventional difference spectra. We shall refer to the two methods as cross-section-weighted (σDS) and chemically weighted difference spectra (CDS), respectively. Figure 15 shows the CDS on the left-hand side and the σDS on the right-hand side for a series of nitrogen concentrations between $x=0.23$ and 2.0. The amplitudes of the spectra before taking the differences were normalized in the region of the background of inelastically scattered electrons and their energies are adjusted using the corelike N 2s level. The energy scales of Fig. 15 are those appropriate for the hydrogenated samples. Also marked are the position of the valence-band maximum and the location of A, B, and C in the unhydrogenated specimens. The results of Fig. 15 may be summarized as follows.

(i) The two kinds of difference spectra are very similar in all essential points, i.e., the positions and shapes of all maxima and minima.

(ii) The incorporation of hydrogen for $x=0.23$ is controlled by the amorphous-silicon network and N—H bonds are of secondary importance. The H 1s—like states H_1 and H_2 occur at energies that correspond to polyhydrides in a-Si. The replacement of Si—Si bonds by the stronger Si—H bonds removes states from the top of the valence bands, as indicated by the negative peak in the difference spectra between the VBM and A. This corresponds to the loss of the shoulder above peak A upon the hydrogenation of a-SiN_x with low x, as shown in Fig. 16 for $x=0.35$ and 0.55. The removal of these states has already been observed in a-Si:H and is responsible for the recession of the VBM and the increase in the optical gap of a-Si:H compared to a-Si.[57,58] The state density at the bottom of the valence bands (excluding the N 2s states for the moment) just below peak C is apparently also reduced, as indicated by the pronounced minimum in the difference

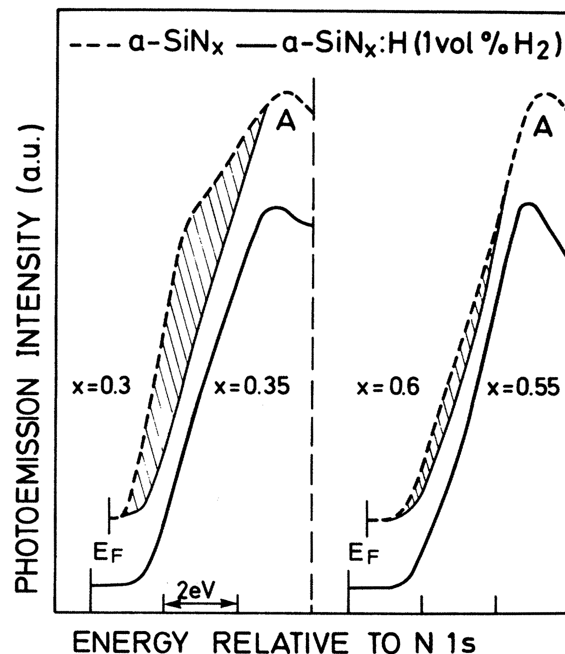

FIG. 16. Comparison of the top of the valence bands for two sputtered a-SiN_x samples with and without hydrogen.

spectra of Fig. 15. These states have a strong Si 3s character (see Fig. 10) and the formation of Si—H bonds pushes these states presumably as Si 3s —H 1s antibonding states up into the conduction bands.

(iii) The difference spectra change gradually from Si—H-dominated ones to spectra where N—H bonds are more frequent. At $x=0.44$ the intensities of H_1 and H_2 are about equal, but the depletion of Si 3p and Si 3s states at top and bottom of the valence bands is still noticeable. For the near stoichiometric $x=1.2$ films, peak H_2 has changed its binding energy by 1.0 eV and, for $x=2.0$, H_2 is the dominant feature in the difference spectra, whereas H_1 is a mere shoulder. Furthermore, the loss of Si 3p and Si 3s states is hardly perceptible any more. Instead, a deep minimum develops between the positions of peaks A and B in the CDS and less pronounced in the σDS. This indicates that Si—N bonding states are now replaced by N—H bonds. The corresponding bonding levels (N—H in Fig. 15) are located at $\sim$10 eV below the VBM—that is, at the bottom of the Si_3N_4 DOS.

(iv) Finally, neither the direct valence-band spectra of a-SiN_x:H in Fig. 13 nor the difference spectra give any indication that the lone-pair peak A is involved in or affected by the incorporation of hydrogen. It remains unaltered in position and intensity and always distinctly separated from the rest of the VB.

F. Position of the VBM and E_F

In Fig. 17 we have plotted the separation between the Fermi level and the VBM as a functoin of nitrogen concentration for all samples investigated. The VBM is determined in the usual way through the extrapolation of the steepest descent of the leading edge of the spectrum to the baseline. E_F-E_{VBM} increases from (0.1 ± 0.1) eV in a-Si (Ref. 58) linearly with x up to (2.2 ± 0.1) eV for stoichiometric a-Si_3N_4, i.e., $x=1.33$. The separation remains unchanged thereafter despite the excess nitrogen concentration. Upon adding hydrogen, the separation increases by an additional 0.5 ($x=1$) to 0.7 eV ($x=0.2$) in sputtered a-SiN_x:H films independent of the H_2 concentration used during deposition. Slightly below stoichiometry, at $x=1.0$, E_F-E_{VBM} levels off at 2.4 eV, which is 0.2 eV higher than in the unhydrogenated samples. Finally, in the heavily hydrogenated specimens, E_F-E_{VBM} starts out with the same value as the other a-SiN_x:H films, rises, however, more rapidly, and reaches its plateau of (3.0 ± 0.1) eV around $x=1.2$. Reducing the hydrogen content of GD a-$SiN_{2.0}$:H by annealing at $T_A=480\,°C$ reduces E_F-E_{VBM} to 2.5 eV, a value that agrees with those found in a-SiN_x:H samples with low hydrogen concentrations ($c_H \leq 10$ at. %).

For an interpretation of the E_F-E_{VBM} values, it is necessary to distinguish between a recession of the VBM and changes in the position of E_F within the forbidden gap. To this end, in Fig. 18 we have plotted the VBM and E_F relative to the energy of the N 1s, level, which does not show any appreciable chemical shifts as discussed in Sec. III A. Two sets of samples are represented in Fig. 18: the unhydrogenated and the heavily hydrogenated glow-discharge specimens. Also included is the position of the conduction-band minimum (CBM) that was obtained by adding our VBM energies to the optical gap E_g obtained by Kurata *et al.*[16] on GD a-SiN_x:H samples prepared at $T_D=300\,°C$ and containing an estimated 14 at. % hydrogen. There is, of course, a considerable uncertainty in this procedure since the VBM and E_g were not measured on the same samples and the hydrogen content differed by at least a factor of 2. It appears, however, that the energy of the CBM is not very sensitive to the hydrogen concentration if the point appropriate for unhydrogenated a-Si_3N_4 that was obtained using $E_g=4.55$ eV from Ref. 59 is sufficient evidence. This would, in fact, be compatible with our observation that the energy of the CBM depends only slightly on hydrogen content in a-Si:H.[58]

The VBM recedes linearly with x up to $x=1.1$ by 1.0 eV since Si—Si bonding states are at the top of the valence bands are successively replaced by stronger Si—N bonds

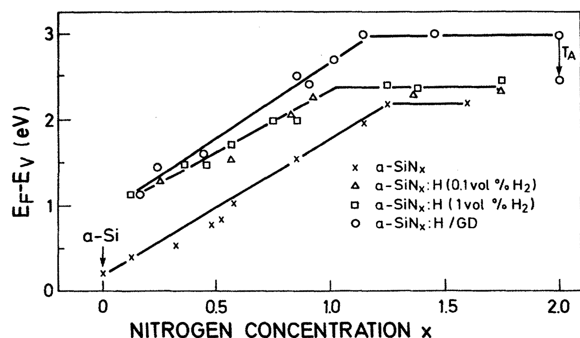

FIG. 17. Separation between E_F and the valence-band maximum (VBM) in all samples investigated as a function of nitrogen concentration.

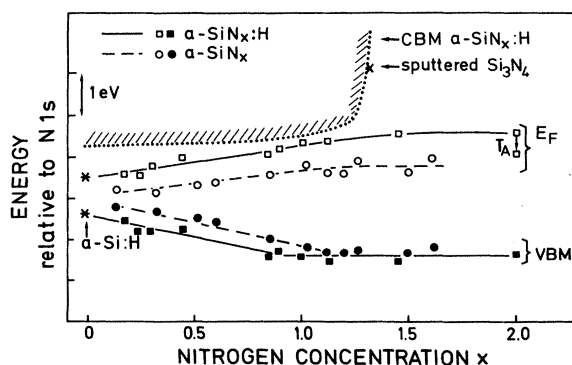

FIG. 18. Position of the VBM and E_F relative to the N 1s core level as a function of nitrogen content for unhydrogenated a-SiN_x and glow discharge a-SiN_x:H. The position of the conduction-band minimum (CBM) was obtained by adding the optical gap of GD a-SiN_x:H ($T_D=300\,°C$) (Ref. 16) to the VBM values of our GD a-SiN_x:H samples. The point $\times$ was derived in the same way using the optical gap of sputtered a-SiN_x without hydrogen (Ref. 59). The energies for a-Si:H (*) are taken from Ref. 58 for a film with comparable hydrogen content ($c_H\sim30$ at. %) using the extrapolation of the VBM (a-SiN_x:H) to $x=0$ as a reference.

with states deeper in the VB, as seen in Fig. 11. The recession stops at $x=1.1$ when the N lone-pair states take over at the top of the valence bands. The addition of hydrogen has the same effect on the VBM: The hydrogen in the GD samples shifts the VBM by an additional 0.3 eV, which is equivalent to a Δx of about 0.2, and thus the recession of the VBM already stops at $x=0.9$ in hydrogenated a-SiN_x:H when all Si—Si bonding states are removed from the TVB.

The Fermi level E_F moves towards the conduction bands when nitrogen is incorporated. E_F starts out within 0.2 eV of the VBM in unhydrogenated a-Si (Ref. 58) and reaches a position within 0.1 eV of the midgap in stoichiometric a-Si_3N_4. Increasing the nitrogen concentration does not shift E_F any further. Adding hydrogen to the specimens, however, moves E_F up between 0.5 and 0.7 eV over the entire range of nitrogen concentrations.

It is well established that small amounts of nitrogen in a-Si:H act as a dopant and lead to an increase in the dark conductivity and photoconductivity.[16,20,30–32] The conductivity is n type and the minimum activation energy of about 0.5–0.6 eV is reached for nitrogen concentrations between $x=0.1$ and 0.2.[16,20,32] This is in agreement with the decreasing separation between the CBM and E_F (a-SiN_x:H) in Fig. 18. From our data we would expect a further decrease in the activation energy for higher nitrogen concentrations, whereas the conductivity drops rapidly beyond $x=0.2$, accompanied by a comparable reduction in the $\eta\mu\tau$ product.[8,20] Since it is unlikely that the number of electron traps changes drastically around $x\cong0.2$, we suggest that the disruption of the a-Si network by an increasing concentration of Si—N bonds reduces the mobility of the charge carriers at the conduction-band edge for $x\cong0.2$ sufficiently to account for the drop in the $\eta\mu\tau$ product. The *position* of the CBM remains comparatively unaffected by the addition of nitrogen as long as Si—Si antibonding states determine the bottom of the conduction states, i.e, up to about $x=1.1$. The increase in the optical gap of SiN_x in this range is determined primarily by the recession of the VBM. Above $x=1.1$ the CBM starts to recede very rapidly. This indicates that the Si—Si antibonding states remaining at the CBM are replaced over a narrow range in x by the much-higher-lying Si—N antibonding states. This implies that a small number of Si—Si bonds give antibonding defect states at an energy which is close to the position of the CBM for $X\lesssim1.1$, i.e., about 3 eV above the VBM in near-stoichiometric a-SiN_x(:H). The rapid increase in the CBM around $x=1.3$ has certain aspects of a percolation threshold: The higher-lying Si—N antibonding states have no influence on the CBM as long as their concentration remains below a critical value. Only when this threshold is reached does the conduction-band edge make a rapid tranistion from Si—Si dominated to Si—N dominated.

Extrapolating the position of the VBM to $x=0$ in Fig. 8, we estimate the valence-band discontinuity between a-Si_3N_4(:H) and a-Si to be (1.5 ± 0.1) eV, and (1.2 ± 0.1) eV between a-Si_3N_4(:H) and a-Si:H. The former value is 0.6 eV lower than the discontinuity between a-Si_3N_4 and c-Si determined by DiMaria and Arnett.[60]

IV. SUMMARY AND CONCLUSIONS

We have analyzed the bonding properties and the electronic structure of amorphous silicon nitride (a-SiN_x) as a function of nitrogen and hydrogen content using high-resolution core-level spectra and valence-band photoemission. Variation in line shape and peak position of the Si $2p$ core-level spectra are explained in terms of a superposition of chemically shifted components that correspond to the different Si valence states associated with the replacement by up to four of the possible Si—Si bonds by Si—N bonds. An analysis of the relative intensities of the different Si—N bonding configurations reveals that nitrogen atoms are almost exclusively incorporated as threefold coordinated by Si atoms for $x\lesssim0.8$. A phase separation into a-Si and stoichiometric a-Si_3N_4 is not observed. Understoichiometric a-SiN_x is thus a random network in which Si—Si bonds are successively replaced by Si—N bonds as required by the $8-N$ rule.

Excess nitrogen, i.e., $x>1.33$, is accommodated by reducing the average Si coordination of the nitrogen atoms. This is presumably accomplished through the formation of N—N bonds or =N defects, i.e., nitrogen atoms with only two Si—N bonds. This kind of undercoordination sets in at around $x=0.9$ for our room-temperature samples. The addition of hydrogen favors undercoordination of nitrogen through the formation of N—H bonds. This has the effect that the average number of N—Si bonds is reduced from three and hydrogenated samples can thus accommodate a much higher nitrogen content (up to $x_{\max}=2.0$) than unhydrogenated samples ($x_{\max}=1.6$).

A band of N $2p$ lone-pair electrons has been identified at the top of the valence bands in stoichiometric and near-stoichiometric a-Si_3N_4. In a-Si the valence-band top is determined by Si $3p$ bonding states. The density of these states is gradually removed by the formation of deeper-lying Si—N bonding states until at $x=1.1$ the N lone-pair states form the valence-band top. This situation prevails up to the highest nitrogen concentrations. The removal of Si $3p$ states at the VB top leads to a recession of the VBM which amounts to 1 eV between $x=0$ and 0.9.

The addition of hydrogen has the same effect as nitrogen insofar as it also removes the Si $3p$ bonding states from the VBM. The 30 to 40 at. % hydrogen in our GD films is equivalent to an increase in the nitrogen concentration of $\Delta x=0.2$. This implies that the transition from Si-derived states at the VBM to N lone-pair electrons occurs in a-SiN_x:H at $x=0.9$ instead of $x=1.1$. Once the N $2p$ lone-pair states have taken over at the VBM, no change in the position or spectral shape of the top 2 eV of the valence bands is observed.

The position of the conduction-band minimum (exhibits a sharp, percolationlike transition at $x_c=1.25$. Below x_c, the CBM is virtually unaffected by the incorporation of nitrogen and its position is that determined by the Si—Si antibonding sates of the a-Si network. The increase in the optical gap in this regime is primarily determined by the recession of the VBM. Above x_c, Si—N antibonding states with their much higher energy take over and the

gap opens up rapidly. We apparently observe here the transition from an amorphous network dominated by the connectivity of the Si—Si bonds to that of the Si—N bonds. It is remarkable that this transition occurs below the stoichiometric nitrogen concentration, but slightly ($\Delta x = 0.3$) above the transition from the Si to the nitrogen-lone-pair—domianted valence-band maximum.

The Fermi level is pinned near the VBM in a-Si and in the center of the gap in a-Si_3N_4. Hydrogen frees E_F to move by 0.5 to 0.7 eV towards the CBM, and since this movement is reversible upon hydrogen evolution it is likely that the pinning is related to Si dangling bonds, in analogy to the situation in a-Si(:H).[58]

We have determined the Si—H and N—H bonding states at 6.3 and 9.8 eV below the VBM in stoichiometric silicon nitride. The relative intensities of these states bears witness to the preferential formation of N—H compared to Si—H bonds.

Finally, we can place, with some confidence, the Si—Si bonding defect states at about 0.5 to 1.0 eV above the VBM in a-SiN_x(:H) and the corresponding antibonding states (3.0 ± 0.3) eV above the VBM for $x > 1.2$. Thus both lie in the gap and are likely candidates for the deep traps responsible for charge storage in MNOS memory devices.

Note added in proof. The density of conduction states and the formation of core excitons in a-SiN_1:H has recently been investigated by the present authors using partial yield spectroscopy [L. Ley, R. Kärcher, and R. L. Johnson, Phys. Rev. Lett. (to be published)].

ACKNOWLEDGMENTS

We are indebted to the HASYLAB team for their hospitality and support during the synchrotron-radiation measurements. We wish to thank Dr. J. Robertson for helpful discussions and for the unpublished partial densities of states. We thank Dr. Kreil for providing us with the stoichiometric silicon nitride calibration sample. The expert technical help of W. Neu and H. Kölln is gratefully acknowledged. This work was supported in part by Der Bundesminister für Forschung und Technologie.

[1]See, e.g., C.-E. Morosanu, Thin Solid Films **65**, 171 (1980).

[2]M. J. Powell, B. C. Easton, and O. F. Hill, Appl. Phys. Lett. **38**, 794 (1981).

[3]J. J. Chang, IEEE Trans. Electron. Devices **ED-24**, 511 (1977), and references therein.

[4]M. Pepper, in *Proceedings of the XXth Conference on Insulating Films on Semiconductors, Bristol,* edited by G. G. Roberts and M. J. Morant (IOP, London, 1980), p. 193, and references therein.

[5]P. C. Arnett and B. H. Yun, Appl. Phys. Lett. **26**, 94 (1975).

[6]R. Hezel and R. Schörner, J. Appl. Phys. **52**, 3076 (1981).

[7]S. Yokoyama, M. Hirose, and Y. Osaka, Jpn. J. Appl. Phys. **20**, L35 (1981).

[8]T. Shimizu, S. Oozora, A. Morimoto, M. Kumeda, and N. Ishii, Solar Energy Mater. **8**, 311 (1982).

[9]G. Sasaki, S. Fujita, and A. Sasaki, J. Appl. Phys. **54**, 2696 (1983).

[10]F. Sequeda and R. E. Richardson, Jr., J. Vac. Sci. Technol. **18**, 362 (1981).

[11]K. Watanabe and S. Wakayama, J. Appl. Phys. **53**, 568 (1982).

[12]J. S. Johannessen, C. R. Helms, W. E. Spicer, and Y. E. Strausser, IEEE Trans. Electron. Devices **ED-24**, 547 (1977).

[13]H. H. Madden, J. Electrochem. Soc. **128**, 625 (1981).

[14]G. Sasaki, M. Kondo, S. Fujita, and A. Sasaki, Jpn. J. Appl. Phys. **21**, 1394 (1982).

[15]S. Fujita, H. Toyoshima, M. Nishihara, and A. Sasaki, J. Electron. Mater. **11**, 795 (1982).

[16]H. Kurata, M. Hirose, and Y. Osaka, Jpn. J. Appl. Phys. **20**, L811 (1981).

[17]P. S. Peercy, H. J. Stein, B. L. Doyle, and S. T. Picraux, J. Electron. Mater. **8**, 11 (1979).

[18]G. Lucovsky, J. Yang, S. S. Chao, J. E. Tyler, and W. Czubatyj, Phys. Rev. B **28**, 3234 (1983).

[19]P. Paduschek and P. Eichinger, Appl. Phys. Lett. **36**, 62 (1980).

[20]G. Sasaki, T. Tanaka, M. Okamoto, S. Fujita, and A. Sasaki, J. Non-Cryst. Solids **59&60**, 597 (1983).

[21]J. Robertson, Philos. Mag. B. **44**, 215 (1981).

[22]J. Robertson, J. Appl. Phys. **54**, 4490 (1983).

[23]S.-Y. Ren and W. Y. Ching, Phys. Rev. B **23**, 5454 (1981).

[24]T. Aiyama, T. Fukunaga, K. Niihara, T. Hirai, and K. Suzuki, J. Non-Cryst. Solids **33**, 131 (1979).

[25]M. Misawa, T. Fukunaga K. Niihara, T. Hirai, and K. Suzuki, J. Non-Cryst. Solids **34**, 313 (1979).

[26]M. Kastner and H. Fritzsche, Philos. Mag. B **37** 199 (1978).

[27]C. T. Kirk, Jr., J. Appl. Phys. **50**, 4190 (1979).

[28]Z. A. Weinberg and R. A. Pollak, Appl. Phys. Lett. **27**, 254 (1975).

[29]D. A. Anderson and W. E. Spear, Philos. Mag. **35**, 1 (1977).

[30]J. Baixeras, D. Mencaraglia, and P. Andro, Philos. Mag. B **37**, 403 (1978).

[31]T. Noguchi, S. Usui, A. Sawada, Y. Kanoh, and M. Kikuchi, Jpn. J. Appl. Phys. **21**, L485 (1982).

[32]H. Watanabe, K. Katoh, and M. Yasui, Thin Solid Films **106**, 263 (1983).

[33]M. V. Coleman and D. J. D. Thomas, Phys. Status Solidi **25**, 241 (1968).

[34]H. R. Philipp, J. Non-Cryst. Solids **8-10**, 627 (1972); J. Electrochem. Soc. **120**, 295 (1973).

[35]R. Kärcher, R. L. Johnson, and L. Ley, J. Non-Cryst. Solids **59&60**, 593 (1983).

[36]R. L. Johnson and J. Reichardt, Nucl. Instrum. Methods **208**, 791 (1983).

[37]K. J. Gruntz, L. Ley, and R. L. Johnson, Phys. Rev. B **24**, 2069 (1981).

[38]I. M. Band, Y. I. Kharitonov, and M. B. Trzhaskovskaya, At. Data Nucl. Data Tables **23**, 443 (1979).

[39]J. H. Scofield, J. Electron. Spectrosc. Relat. Phenom. **8**, 129 (1976).

[40]U. Gelius, P.-F. Hedén, J. Hedman, B. J. Lindberg, R. Manne, R. Nordberg, C. Nordling, and K. Siegbahn, Phys. Scr. **2**, 70 (1970).

[41]P. Kelve, B. Blomster, H. Siegbahn, K. Siegbahn, E. Sanhueza, and O. Goscinski, Phys. Scr. **21**, 75 (1980).

[42]R. N. Nucho and A. Madhukar, in *The Physics of* SiO_2, edited by S. T. Pantelides (Pergamon, New York, 1978), p. 60.

[43] F. J. Grunthaner and J. Maserjian, in *The Physics of SiO_2*, Ref. 42, p. 389.
[44] L. Ley, J. Reichardt, and R. L. Johnson, Phys. Rev. Lett. **49**, 1664 (1982).
[45] G. Hollinger, Appl. Surf. Sci. **8**, 318 (1981).
[46] Y. Katayama, K. Usami, and T. Shimada, Philos. Mag. B **43**, 283 (1981).
[47] L. Ley, in *The Physics of Amorphous Silicon*, edited by J. D. Joannopoulos and G. Lucovsky (Springer, Heidelberg, 1984), Vol. II, p. 61.
[48] A. K. Sinha, H. J. Levinstein, T. E. Smith, G. Quintana, and S. E. Haszko, J. Electrochem. Soc. **125**, 601 (1978).
[49] M. Nishijima and K. Fujiwara, Solid State Commun. **24**, 101 (1977).
[50] R. Hezel and N. Lieske, J. Appl. Phys. **53**, 1671 (1982).
[51] J. Robertson (private communication).
[52] S. M. Goldberg, C. S. Fadley, and S. Kono, J. Electron. Spectrosc. Relat. Phenom. **21**, 285 (1981).
[53] B. Fischer, R. A. Pollak, T. H. DiStefano, and W. D. Grobmann, Phys. Rev. B **15**, 3193 (1977).
[54] B. von Roedern, L. Ley, M. Cardona, and F. W. Smith, Philos. Mag. B **40**, 433 (1979).
[55] T. Isu and K. Fujiwara, Solid State Commun. **42**, 477 (1982).
[56] M. Hundhausen, J. Non-Cryst. Solids **59&60**, 601 (1983).
[57] R. Kärcher and L. Ley, Solid State Commun. **43**, 415 (1982).
[58] J. Reichardt, L. Ley, and R. L. Johnson, J. Non-Cryst. Solids **59&60**, 329 (1983).
[59] J. Bauer, Phys. Status Solidi A **39**, 411 (1977).
[60] D. J. DiMaria and P. C. Arnett, Appl. Phys. Lett. **26**, 711 (1975).